BIOCHEMISTRY
including biophysical chemistry & molecular biology

Article

pubs.acs.org/biochemistry

Characterization of AusA: A Dimodular Nonribosomal Peptide Synthetase Responsible for the Production of Aureusimine Pyrazinones

Daniel J. Wilson,[†] Ce Shi,[†] Aaron M. Teitelbaum,[‡] Andrew M. Gulick,[§] and Courtney C. Aldrich*[,†]

[†]Center for Drug Design, University of Minnesota, Minneapolis, Minnesota 55455, United States

[‡]Department of Medicinal Chemistry, University of Minnesota, Minneapolis, Minnesota 55455, United States

[§]Hauptman-Woodward Institute and Department of Structural Biology, University at Buffalo, Buffalo, New York 14203, United States

Supporting Information

ABSTRACT: Aureusimines have been identified as potential virulence factors in *Staphylococcus aureus*. These pyrazinone secondary metabolites are produced by a nonribosomal peptide synthetase (NRPS) annotated as AusA. We report the overproduction of AusA as a 277 kDa soluble protein with A_1–T_1–C–A_2–T_2–R bimodular architecture. The substrate specificity of each adenylation (A) domain was initially probed using an ATP–pyrophosphate exchange assay with A-domain selective bisubstrate inhibitors to chemically knock out each companion A-domain. The activity of AusA was then reconstituted in vitro and shown to produce all naturally occurring aureusimines and non-natural pyrazinone products with k_{cat} values ranging from 0.4 to 1.3 min^{-1}. Steady-state kinetic parameters were determined for all substrates and cofactors, providing the first comprehensive steady-state characterization of a NRPS employing a product formation assay. The K_M values for the amino acids were up to 60-fold lower with the product formation assay than with the ATP–pyrophosphate exchange assay, most commonly used to assess A-domain substrate specificity. The C-terminal reductase (R) domain catalyzes reductive release of the dipeptidyl intermediate, leading to formation of an amino aldehyde that cyclizes to a dihydropyrazinone. We show oxidation to the final pyrazinone heterocycle is spontaneous. The activity and specificity of the R-domain was independently investigated using a NADPH consumption assay. AusA is a minimal autonomous two-module NRPS that represents an excellent model system for further kinetic and structural characterization.

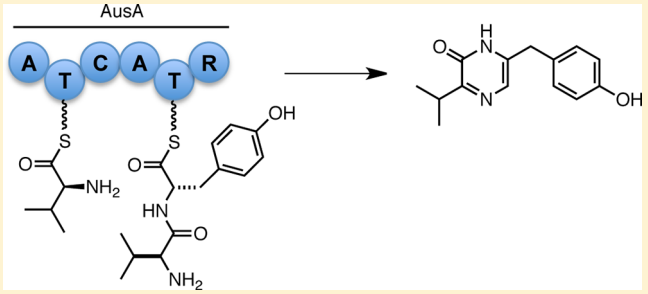

The aureusimines are cyclic dipeptide pyrazinone natural products produced by *Staphylococcus aureus*, a significant human pathogen,[1] that were independently discovered by the Magarvey and Fischbach research groups.[2,3] Genomic mining of all sequenced *S. aureus* strains (>50) revealed a conserved gene cluster encoding two genes (*ausA* and *ausB*), whose linkage to aureusimine biosynthesis was confirmed through genetic inactivation by allelic replacement. Aureusimines appear to play a role in virulence as the expression of a wide variety of genes is modulated in a Δ*ausA* mutant, including γ-hemolysin, superantigen-like genes, and several respiratory metabolic genes.[4] However, the initially reported gene expression profile of the Δ*ausA* mutant[2] was largely caused by an inadvertent secondary mutation in *saeS*, part of a two-component regulator in *S. aureus* that controls virulence factor expression.[5] Although the biological role of the aureusimines remains unknown, they are expected to have an important function given the conservation of their gene cluster among *S. aureus* isolates coupled with the recent findings that they are overproduced in *S. aureus* biofilms.[6]

Aureusimine dipeptides are biosynthesized through a nonribosomal peptide synthetase (NRPS) pathway (Figure 1). NRPSs are multifunctional proteins that synthesize peptide natural products in a manner independent of the mRNA ribosomal machinery and employ a modular architecture wherein each module is responsible for the incorporation of one amino acid into the final peptide product.[7,8] The canonical module contains three core domains: an adenylation domain (A-domain) responsible for the selection and activation of an amino acid,[9] a thiolation domain (T-domain) onto which the amino acid is covalently tethered as a thioester to the terminal thiol of the 4′-phosphopantetheine prosthetic group,[10] and a condensation domain (C-domain), which catalyzes peptide bond formation in the N to C direction between the upstream and downstream aminoacyl thioesters. Release of the nascent peptide from the NRPS assembly line is often accompanied by cyclization through the activity of a thioesterase (TE) domain

Received: September 29, 2012
Revised: December 21, 2012
Published: January 9, 2013

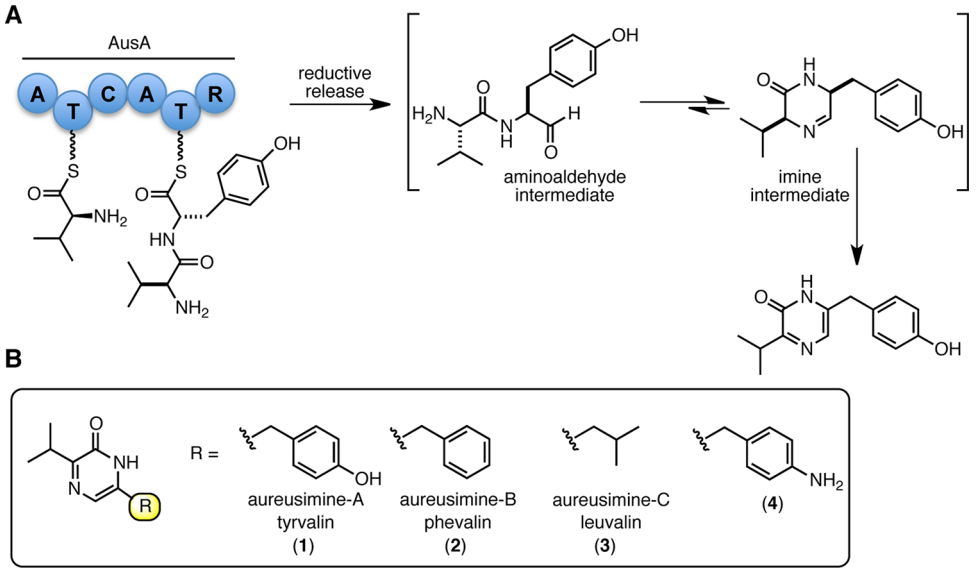

Figure 1. (A) Biosynthetic pathway of the aureusimines. (B) Aureusimines and related pyrazinones described in this work.

Table 1. Oligonucleotide Primers

Primer name	primer direction	primer sequence	domains
ausA F1	5'-forward	ATTTTCAGGGCCATATGAAAGAAGGACTTTTTATG	his-A1-T1-C-A2-T2-R
ausA R1	3'-reverse	TTCTCCAGGAATACCAACGC	his-A1-T1-C-A2-T2-R
ausA F2	5'-forward	GCGTTGGTATTCCTGGAGAA	his-A1-T1-C-A2-T2-R
ausA R2	3'-reverse	TGCGAGACAACTAACATCGC	his-A1-T1-C-A2-T2-R
ausA F3	5'-forward	GCGATGTTAGTTGTCTCGCA	his-A1-T1-C-A2-T2-R
ausA R3	3'-reverse	GTGCGGCCGCAAGCTTACTTATTGAATATTGTTTTGATATATTGTG	his-A1-T1-C-A2-T2-R
ausA 1st AT R	3'-reverse	GTGCGGCCGCAAGCTTAAACTATAGTTTCTGGAATCACTTC	his-A1-T1
ausA 2nd AT F	5'-forward	ATTTTCAGGGCCATATGCCAAACGGCACGGAGGAAC	his-A2-T2-R

or more rarely by a reductase (R) domain.[11] Aureusimine synthesis requires two proteins: AusA encodes a two-module six-domain NRPS, with $A_1-T_1-C-A_2-T_2-R$ domain architecture, while AusB encodes a phosphopantetheinyl transferase responsible for posttranslational modification of apo-AusA through attachment of 4′-phosphopantetheine onto a conserved serine residue of both T-domains. Bioinformatic analysis suggests the first adenylation domain (A_1) specifies for valine while the second adenylation domain (A_2) is predicted to confer specificity for tyrosine.[2] Thus, A_1 activates and loads T_1 with L-valine to afford L-Val-S∼T_1, and A_2 activates and loads T_2 with L-tyrosine to afford L-Tyr-S∼T_2. The condensation domain (C) then catalyzes peptide bond formation to afford the dipeptide L-Val-L-Tyr∼T_2, which is reduced by the R-domain to afford an intermediate amino aldehyde that cyclizes to an imine. Oxidation to the pyrazinone is proposed to occur spontaneously, driven by the greater stability associated with aromatization or alternatively catalyzed by an oxidoreductase.[3] The isolation of multiple pyrazinone products containing L-Tyr, L-Phe, and L-Leu suggests A_2 has relaxed substrate specificity.

Unlike most NRPS pathways that require multiple NRPS proteins for assembly of their respective natural product, AusA is predicted to autonomously synthesize the aureusimines. Therefore, AusA represents an excellent model system for structural and kinetic studies as well as for investigating NRPS protein engineering because it is a minimal canonical NRPS. Although several natural two-module NRPSs have been reported, including LtxA that is involved in biosynthesis of the lyngbyatoxin NRPs,[12] AnaPS from the acetylaszonalenin indole alkaloid pathway,[13] and FtmA that catalyzes diketopiperazine formation of the fumitremorgins,[14] none have been biochemically characterized.

Herein we describe the expression and functional characterization of AusA, an approximately 280 kDa protein. The substrate specificity of each A-domain is determined with a large panel of natural and non-natural amino acids employing A-domain selective inhibitors to knock out the activity of the other A-domain. The activity of AusA is successfully reconstituted in vitro and shown to produce the naturally occurring aureusimines as well as unnatural pyrazinones. A product formation assay is developed and used to evaluate the steady-state kinetic parameters for all substrates and cofactors. Finally, we demonstrate oxidation of the initially formed imine intermediate to the pyrazinone is spontaneous and also examine the specificity of release by the R-domain. During review of the manuscript, Magarvey reported the expression and in vitro reconstitution of AusA as well as the structural characterization of the R-domain.[15]

MATERIALS AND METHODS

Materials. The following materials were purchased from the indicated supplier: chemically competent *Escherichia coli* Mach1 and BL21 STAR(DE3) cells (Invitrogen, Carlsbad, CA), In-Fusion cloning kit (Clonetech, Mountain View, CA), restriction enzymes (New England Biolabs, Ipswich, MA), PrimeSTAR HS DNA polymerase (TAKARA Bio Inc., Otsu, Shiga, Japan), primers for polymerase chain reaction (PCR) (Integrated DNA Technologies, Coralville, IA), Ni-NTA, and DNA purification/

dx.doi.org/10.1021/bi301330q | *Biochemistry* 2013, 52, 926−937

isolation kits (Qiagen Sciences, Germantown, MD), ion exchange and gel filtration columns (GE healthcare, Waukesha, WI), NADPH and ATP as well as all biological buffers and components (Sigma-Aldrich, St. Louis, MO), amino acids (Chem-Impex, Wood Dale, IL), and radioactive [^{32}P]-pyrophosphate (PerkinElmer, Waltham, MA).

Cloning and Expression of AusA. The *ausA* gene was amplified by PCR from *S. aureus* ATCC 43300 in three fragments using the following primer pairs: ausA F1 and ausA R1, ausA F2 and ausA R2, and ausA F3 and ausA R3 (Table 1). The three fragments were ligated into *Nde*I- and *Hin*dIII-digested pET28b-TEV, an expression vector with the thrombin cleavage site replaced with a TEV cleavage site, using the In-Fusion PCR cloning kit (Clontech) following the manufacturer's instructions. The final construct, pCDD141, expresses AusA with an N-terminal hexahistidine tag (276.6 kDa). Sequencing revealed the expression plasmid to be error free. Similarly, the A_1-T_1 didomain was amplified using primers ausA F1 and ausA first AT R (amino acids 1−999), and the A_2-T_2-R tridomain (amino acids 1418−2397) was amplified using ausA second AT F and ausA R3. Both PCR products were cloned into pET28b-TEV as described above, yielding pCDD142 and pCDD143, respectively.

For expression and purification of apo-AusA, pCDD141 was transformed into *E. coli* BL21(DE3) cells. Overnight cultures (1%) were used to inoculate 1 L of TB medium supplemented with 50 μg/mL kanamycin. Cultures were allowed to grow to an A_{600} of 0.6 at 37 °C, then induced with 0.4 mM IPTG, and allowed to grow for 16 h at 18 °C. Cells were pelleted by centrifugation at 5000*g* for 10 min and resuspended in lysis buffer [50 mM HEPES, 300 mM NaCl, and 10 mM imidazole (pH 8.0)]. Cells were lysed on a Branson model 250 sonifier using five 2 min bursts, at power level 8 with a 30% duty cycle. The lysate was centrifuged at 45000*g* for 10 min at 4 °C. The cleared lysate was incubated with 0.5 mL of Ni-NTA (Qiagen) for 1 h at 4 °C and then loaded onto a gravity column. The Ni-NTA column was washed with 16 mL of wash buffer [50 mM HEPES, 300 mM NaCl, and 20 mM imidazole (pH 8.0)] followed by elution with 3 mL of elution buffer [50 mM HEPES, 300 mM NaCl, and 250 mM imidazole (pH 8.0)]. The eluent was diluted to 4.5 mL with water and then further purified using a MonoQ 5/50 GL strong anion exchange column (GE Life Sciences) running a linear gradient from 0 to 1 M NaCl in 20 mM Tris (pH 8.0) over 40 column volumes at a rate of 1.5 mL/min. The fractions containing AusA were pooled and run on a HiPrep 16/60 Sephacryl S-200 gel filtration column (GE Life Sciences) running 10 mM Tris (pH 8.0) and 200 mM NaCl isocratically. Purified AusA was pooled; glycerol was added to a final concentration of 5%, and the protein was stored at −80 °C. The A_1-T_1 didomain and A_2-T_2-R tridomain were expressed using an identical protocol to afford 16.7 and 20.0 mg/L, respectively. Holo-AusA was expressed and purified as described above except pCDD141 was transformed into *E. coli* BL21(DE3) cells containing pSFP, a plasmid that constitutively expresses the promiscuous phosphopantetheinyl transferase from *Bacillus subtilis*. The yield for both apo- and holo-AusA was 0.5 mg/L. All media used were supplemented with 25 μg/mL chloramphenicol to maintain pSFP.

ATP−PP$_i$ Exchange Assay for AusA A-Domain Substrate Specificity. All reactions were conducted in duplicate under initial velocity conditions in a final volume of 100 μL. The counts from the bound [^{32}P]ATP were converted into product concentration using a standard curve of [^{32}P]-pyrophosphate. To determine the substrate specificity of each adenylation domain in AusA, the following L-amino acids (Ala, Arg, Asp, Cys, Gln, Glu, Gly, His, Ile, Leu, Cle, Tle, Lys, Met, Phe, 4Aph, β-Aph, Pro, Trp, and Val), each at 30 mM, or 10 mM L-Tyr was individually added to a reaction mixture containing 36 nM apo-AusA and 3 mM ATP in ATP−PP$_i$ assay buffer [375 mM Bicine (pH 8.0), 10 mM $MgCl_2$, 2 mM DTT, 1 mM pyrophosphate, and 0.25 μCi of [^{32}P]pyrophosphate]. The reaction mixtures were incubated at 37 °C for 20 min and then quenched with 200 μL of quenching buffer (350 mM perchloric acid, 100 mM PP$_i$, and 1.6% activated charcoal). Excess [^{32}P]pyrophosphate was removed after centrifugation by washing the charcoal with 500 μL of water. The washed pellet was transferred with 200 μL of water to a scintillation vial, and 5 mL of scintillation fluid (RPI) was added. Radioactive counts were quantitated on a Packard Tri Carb 2900 TR instrument. Substrates that showed activity were rerun in the presence of 100 μM Phe-AMS or Val-AMS.

The kinetic constants for the A_1 domain for L-Val and L-Ile were determined as described above using 18 and 36 nM apo-AusA, respectively. The substrate acid concentrations were varied from 41.2 μM to 30 mM using a 3-fold dilution series at a fixed concentration of ATP (3 mM). The substrates for the A_2 domain were similarly tested using the indicated concentration ranges of L-4Aph (41.2 μM to 30 mM), L-Tyr (41.2 μM to 10 mM), L-Leu (123.4 μM to 30 mM), and L-Phe (41.2 μM to 30 mM) at a fixed concentration of ATP (3 mM) using 36 nM apo-AusA for L-Tyr and 72 nM apo-AusA for the remaining substrates. The kinetic parameters for ATP were evaluated at a fixed saturating concentration of L-Phe (30 mM) with 36 nM apo-AusA an ATP concentration varying from 13.7 μM to 10 mM. Individual substrate saturation kinetic data were fit by nonlinear regression analysis to either the Michaelis−Menten equation (eq 1) or the substrate inhibition model (eq 2) using GraphPad Prism 5.0.

$$v = \frac{V_{max}[S]}{K_m + [S]} \quad (1)$$

$$v = \frac{V_{max}[S]}{K_m + [S]\left(1 + \frac{[S]}{K_i}\right)} \quad (2)$$

Determination of the Inhibition Constants of Val-AMS and Phe-AMS. Inhibitors against the two AusA adenylation domains were analyzed using the ATP−PP$_i$ exchange assay under initial velocity conditions to determine the apparent inhibition constants (appK_i). Evaluation of Val-AMS was performed with 10.5 nM apo-AusA, 3 mM L-Val, and 3 mM ATP in ATP−PP$_i$ assay buffer and Val−AMS concentrations varying from 6.25 to 400 nM using a 2-fold dilution series. Evaluation of Phe-AMS was performed with 21 nM apo-AusA, 1 mM L-Tyr, 3 mM ATP in ATP−PP$_i$ assay buffer, and Phe-AMS concentrations varying from 3.1 to 200 nM using a 2-fold dilution series. Inhibition studies with the A_1-T_1 didomain employed 36 nM enzyme, 1 mM L-Val, and 3 mM ATP in ATP−PP$_i$ assay buffer. Inhibition studies with the A_2-T_2-R tridomain employed 360 nM enzyme, 1 mM L-Tyr, and 3 mM ATP in ATP−PP$_i$ assay buffer. Fractional initial velocities were fit by nonlinear regression analysis to the Morrison equation (eq 3) using GraphPad Prism 5.0:

$$\frac{v_i}{v_0} = 1 - \left[[E] + [I] + \text{app}K_i - \sqrt{([E] + [I] + \text{app}K_i)^2 - 4[E][I]} \right] / \left(2[E] \right) \quad (3)$$

where [I] represents the inhibitor concentration, appK_i is the apparent inhibition constant, [E] is the active enzyme concentration (determined by active site titration), v_i is the initial rate at each [I], and v_0 is the initial rate of the DMSO control.

Reconstitution of AusA Activity and Spontaneous Oxidation To Provide Aureusimine-B (2). Reconstitution of AusA activity was initially performed in a 600 μL reaction mixture with 40 nM holo-AusA, 25 mM L-Val, 25 mM L-Phe, 3 mM ATP, and 0.1 mM NADPH in reaction buffer [375 mM Bicine (pH 8.0), 3 mM $MgCl_2$, and 1 mM TCEP]. The reaction mixture was incubated at 37 °C for 3 h. The enzyme was removed by passing the mixture through an Amicon Ultra 10000 molecular weight cutoff filter. The filtrate was collected and incubated at 100 °C for 0−30 min and then analyzed by HPLC. The separation of **2** was performed on an Agilent model 1100 liquid chromatograph system using a Zorbex Eclipse XDB-C8 150 mm × 3.0 mm, 3.5 μm column. Aureusimine-B (**2**) eluted at 6.35 min using an isocratic method with 35% acetonitrile and 65% water containing 0.05% formic acid at a flow rate of 0.5 mL/min. The product was detected with a fluorescence detector measuring excitation at 320 nm and emission at 390 nm and quantitated using a standard curve of authentic aureusimine-B (**2**).

Kinetic Characterization of AusA Using the Product Formation Assay. Reactions were conducted under initial velocity conditions. Reaction mixtures (100 μL final volume) were assayed using 40 nM holo-AusA in 375 mM Bicine (pH 8.0), 10 mM $MgCl_2$, and 1 mM TCEP. Kinetic parameters for the varied substrate used a 2-fold dilution series over the indicated concentration range with fixed concentrations of the remaining substrates at the indicated concentration. Experiments with ATP (13.7 μM to 10 mM) included 100 μM NADPH, 5 mM L-Val, and either 10 mM L-4Aph, 10 mM L-Tyr, 30 mM L-Leu, or 10 mM L-Phe. Experiments with L-4Aph (13.7 μM to 30 mM), L-Tyr (4.6 μM to 10 mM), L-Leu (13.7 μM to 30 mM), and L-Phe (4.6 μM to 10 mM) included 3 mM ATP, 100 μM NADPH, and 5 mM L-Val. Experiments with L-Val (2.3 μM to 5 mM) included 3 mM ATP, 100 μM NADPH, and 1 mM L-Tyr. Experiments with NADPH (1.4 μM to 1 mM) included 3 mM ATP, 5 mM L-Val, and either 30 mM L-4Aph, 10 mM L-Tyr, 30 mM L-Leu, or 10 mM L-Phe. Reaction mixtures were incubated at 37 °C for 2.5 h and then inactivated at 100 °C for 20 min. For experiments with ATP, amino acids (except L-Val), and NADPH, the quenched reaction mixtures containing the same concentration of the varied substrate were pooled before analysis by LC−MS to allow for the simultaneous quantification of each of the four measured products. To accurately determine the concentration of holo-AusA, the enzyme was titrated with Phe-AMS (3.1−400 nM) using 200 nM holo-AusA, 3 mM L-Val, 0.2 mM L-Tyr, 0.2 mM ATP, and 0.1 mM NADPH.

LC−MS Analysis of AusA Reaction Products. LC−MS/MS was performed on a Shimadzu HPLC system coupled with an AB SCIEX QTRAP 5500 mass spectrometer. Samples were analyzed with an electrospray source run in the positive mode. Source and gas parameters were set to the following: curtain gas, 40; CAD gas, medium; ion spray voltage, 3000 V; temperature, 600 °C; gas 1, 45; gas 2, 40. Pyrazinones, tyrosinol, and tyrosinal oxime were analyzed using multiple-reaction monitoring (MRM) using the parameters listed in Table 2.

Table 2. MS Parameters for Detection of Pyrazinone Products

pyrazinone	precursor mass (Da)	product mass (Da)	dwell time (ms)	DP[a]	EP[b]	CE[c]	CXP[d]
1	245.2	136.1	100	100	10	39	17
2	229.1	100	100	100	10	27	16
3	195.1	137.1	100	100	10	37	17
4	244.1	151.2	100	100	10	27	20
tyrosinol (**S8**)	168.1	107	100	60	10	22	14
tyrosinal oxime (**S10**)	361	181.1	100	130	10	47	23

[a]Declustering potential. [b]Entrance potential. [c]Collision energy. [d]Collision cell exit potential.

The samples were separated using a 50 mm × 2.0 mm Varian Polaris C-18 column (5 μm) with a mobile phase of 0.1% aqueous formic acid (mobile phase A) and acetonitrile containing 0.1% formic acid (mobile phase B) with a flow rate of 0.5 mL/min. Products were eluted after being run isocratically with mobile phase A for 0.2 min followed by a linear gradient of 0 to 95% mobile phase B for 1.5 min. Subsequently, the column was washed with mobile phase B (95%) for 1.2 min and reequilibrated with mobile phase A (100%) for 4 min. Pyrazinone products **1**−**4** eluted at 1.6, 2.3, 1.8, and 2.1 min, respectively. Tyrosinol **S8** and tyrosinal oxime **S10** eluted at 0.76 and 1.59 min, respectively (see the Supporting Information for structures).

For the identification of tyrosinal, the aldehyde was converted to a pentafluorobenzyl oxime following the protocol of Li and co-workers.[16] Briefly, reaction mixtures were extracted three times with ethyl acetate. The extract was then dried to completion and resuspended in 100 μL of methanol. Pentafluorobenzyl hydroxylamine (Sigma) was added to the extract (5 μL of a 10 mg/mL solution) and allowed to react at room temperature for 3 h. The solution was diluted with 3 volumes of 0.1% formic acid and analyzed as described above using LC−MS.

Each LC−MS run was exported into MultiQuant (AB SCIEX), which calculated the concentration of each peak using a standard curve of the six synthesized standards (2.7 nM to 2 μM) that was run with each experiment. The concentration of product was transformed into v_i, values and the saturation curves were a fit to either eq 1 or 2.

NADPH Consumption Assay. The reductase domain activity was independently investigated by monitoring the consumption of NADPH by following the change in absorbance at 360 nm on a Molecular Devices M5e multimode plate reader. Assays were set up in duplicate and contained 80 nM holo-AusA in reaction buffer [375 mM Bicine (pH 8.0), 3 mM $MgCl_2$, 3 mM ATP, and 1 mM TCEP] containing 100 μM NADPH and either 1 mM L-Tyr, 1 mM L-Val, or both amino acids. Reactions were monitored continuously at ambient temperature for 45 min. The extinction coefficient of NADPH

(ε_{340} = 6220 M^{-1} cm^{-1}) was used to convert slopes into activity. The reaction solutions were then transferred into individual tubes, and the reaction products were analyzed by LC−MS as described above.

RESULTS

Cloning and Expression of AusA Constructs. AusA was cloned directly from three PCR fragments into an expression vector in a single step using Clonetech's In-Fusion system and confirmed by sequencing the whole gene for PCR errors. This strategy greatly increased the efficiency of cloning such a large construct (7.2 kb) and avoided the necessity of utilizing compatible restriction enzymes, which can be quite challenging for large inserts. AusA was expressed as the full-length apoprotein containing an N-terminal six-His tag in *E. coli* at 18 °C via induction with 0.4 mM IPTG. Initial expression profiling showed that a significant amount of proteolysis occurs near the N-terminus during induction. Consequently, we found the N-terminus was a superior location for the six-His tag as the smaller six-His-tagged fragments were easily separated by gel filtration. We also attempted to purify a doubly tagged protein with an N-terminal six-His tag and a C-terminal Strep tag, but the yield was not improved (data not shown). The 277 kDa AusA protein was purified by sequential nickel affinity chromatography, ion exchange, and gel filtration to afford approximately 0.5 mg/L of culture at >90% purity. The A_1−T_1 didomain and A_2−T_2−R tridomain [attempts to prepare an A_2−T_2 didomain were unsuccessful (data not shown)] were also cloned and expressed using similar methods.

Adenylation Domain Specificity. The two adenylation domains in full-length AusA were initially probed using the classic ATP−[^{32}P]pyrophosphate (PP_i) exchange assay. Twenty-two natural and non-natural L-amino acids were screened for activity against AusA (Figure 3A). In addition to known substrates L-Val, L-Leu, L-Phe, and L-Tyr, we also identified seven other amino acids whose activity was above background, including 4-aminophenylalanine (L-4Aph), L-Ile, cycloleucine (L-Cle), and *tert*-butylleucine (L-Tle).

To distinguish the substrate specificity of each A-domain, we used small molecule bisubstrate inhibitors initially described for the functionally related aminoacyl tRNA synthetases[17] to "chemically knock out" each A-domain and then tested the activity of the other A-domain. We synthesized 5′-*O*-[*N*-(valinyl)sulfamoyl]adenosine (Val-AMS) and 5′-*O*-[*N*-(phenylalanyl)sulfamoyl]adenosine (Phe-AMS) (Figure 2B) as inhibitors of A_1 and A_2, respectively. These inhibitors mimic the intermediate acyl-adenylate formed in the A-domain adenylation half-reaction by replacement of the labile acyl phosphate moiety with a chemically stabile acyl sulfamate isostere and derive their binding affinity through simultaneous interaction with the amino acid and ATP binding pockets.[17] We evaluated the apparent inhibition constants of Val-AMS and Phe-AMS using the ATP−PP_i exchange assay by measuring the initial rates (v_0) at various inhibitor concentrations ([I]) at fixed substrate concentrations.[18] Because of the tight-binding nature of both inhibitors, the resulting concentration−response plots were fit to the Morrison equation (eq 3, Materials and Methods) to provide apparent K_i values of 44 and 0.8 nM for Val-AMS and Phe-AMS, respectively (Figure 2A and Table 3).[19] To confirm the inhibitor selectivity, we also measured the apparent K_i values of each inhibitor against the individual apo-A−T di- and apo-A−T−R tridomain constructs (Table 3). Val-AMS exhibits potent inhibition of the A_1−T_1 didomain but unexpectedly shows modest inhibition of the A_2−T_2−R tridomain with an appK_i of 10 μM, providing a selectivity factor of 158 [i.e., $K_i^{(A_2-T_2-R)}/K_i^{(A_1-T_1)}$]. Conversely, Phe-AMS is a potent inhibitor of the A_2−T_2 didomain with an appK_i of <4 nM and displays little inhibition of the A_1−T_1 didomain even up to 100 μM, providing a selectivity factor of >10^4. These results confirm the high specificity of these inhibitors for their cognate A-domains. The residues predicted to form the valine binding pocket in the A_1 domain are highly conserved with the active site of PA1221, an A−T didomain NRPS protein that was recently crystallized in the presence of a valine-adenosine vinylsulfonamide inhibitor.[20] A sequence comparison shows that only one residue, which is ~7 Å from the valine side chain, is different between the two sequences (Figure S1 of the Supporting Information).

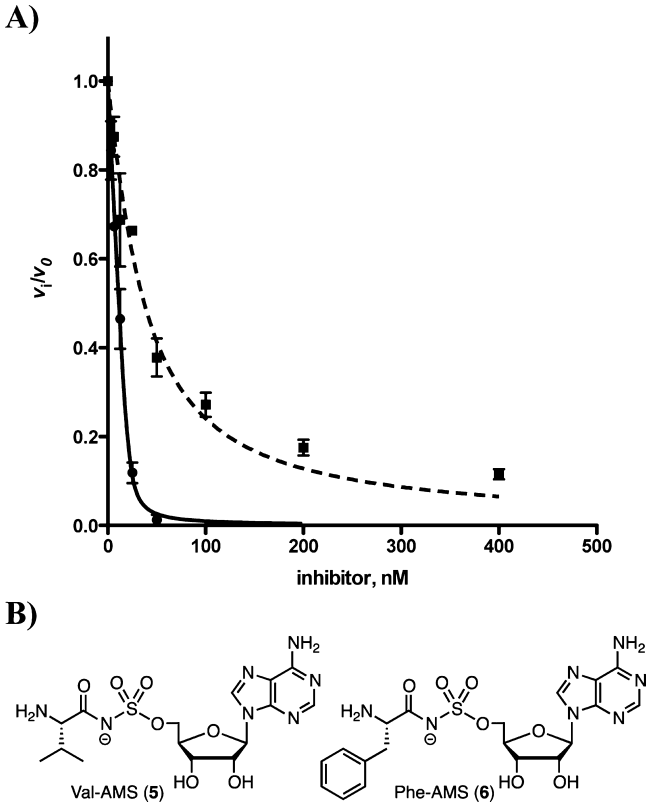

Figure 2. (A) Concentration−response plot of the fractional initial velocity of [^{32}P]ATP formation catalyzed by AusA as a function of Phe-AMS concentration (—) and Val-AMS (---). The curve represents the best nonlinear fit of the data to the Morrison equation. The data points represent the mean with the standard error of duplicate experiments. (B) Structures of Val-AMS and Phe-AMS.

Table 3. Inhibition Constants of Val-AMS and Phe-AMS with AusA and Individual A−T Constructs

	appK_i (nM)	
protein	Val-AMS	Phe-AMS
AusA (A_1−T_1−C−A_2−T_2−R)	44 ± 7	0.8 ± 0.5
A_1−T_1	63 ± 5	>10^5
A_2−T_2−R	(10 ± 1) × 10^3	<4[a]

[a]Because of the lower activity of the A_2−T_2−R tridomain, larger amounts of protein were required, resulting in protein titration, and thus, we are able to calculate only a lower limit for appK_i.

dx.doi.org/10.1021/bi301330q | *Biochemistry* 2013, 52, 926−937

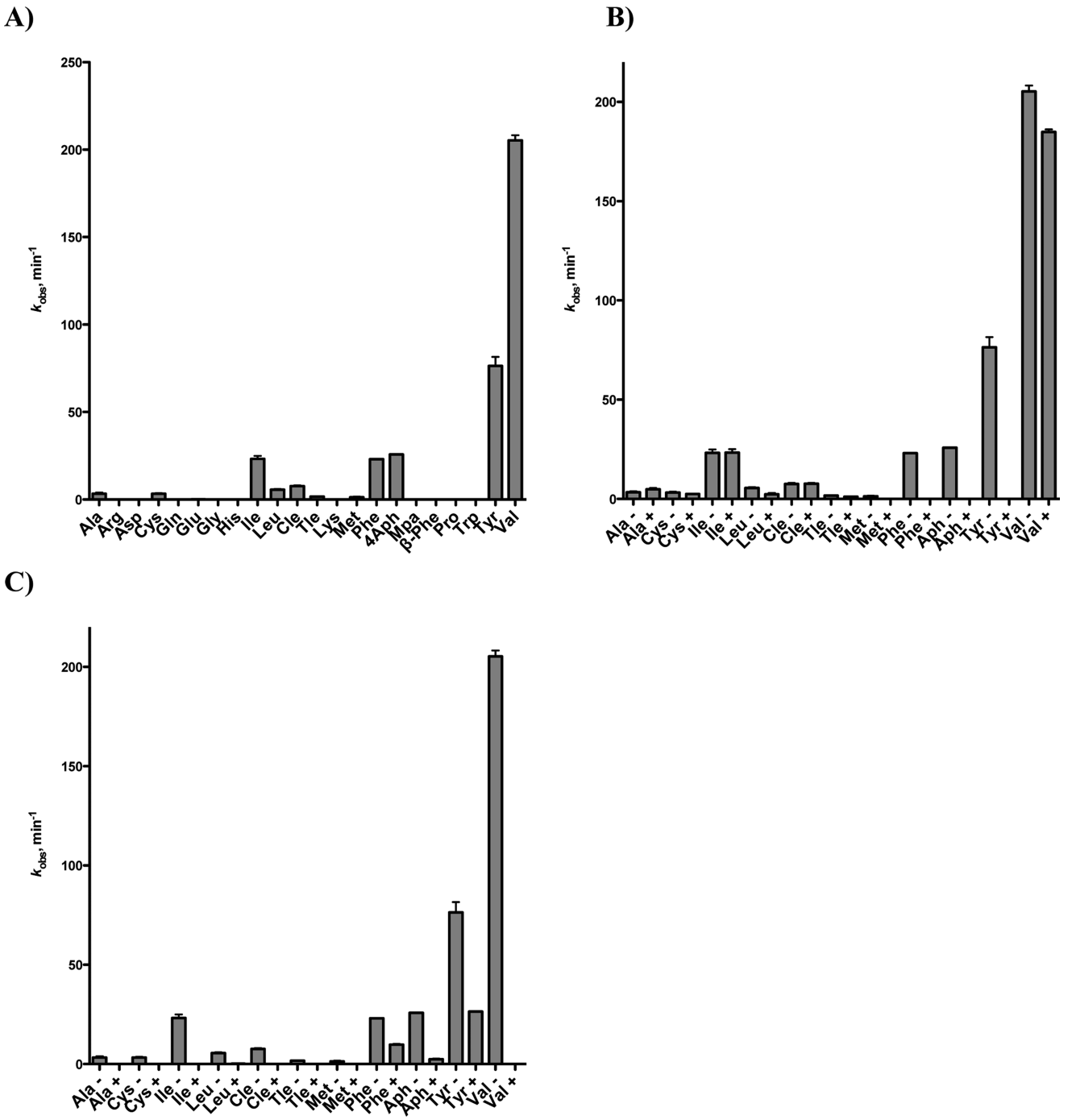

Figure 3. Substrate specificity of AusA using the pyrophosphate exchange assay. Each reaction mixture contained 36 nM apo-AusA, 375 mM Bicine (pH 8.0), 10 mM $MgCl_2$, 3 mM ATP, 2 mM DTT, 1 mM pyrophosphate, 0.25 μCi of [^{32}P]pyrophosphate, and the selected amino acid (30 mM) except for tyrosine, the concentration of which was held at 10 mM. Nonstandard amino acid abbreviations: Cle, L-cycloleucine; Tle, L-*tert*-leucine; 4Aph, L-4-aminophenylalanine; Mpa, α-methylphenylalanine; β-Phe, β-aminophenylalanine: (A) no inhibitor, (B) without (−) or with (+) 100 μM Phe-AMS, and (C) without (−) or with (+) 100 μM Val-AMS.

Each of the 11 amino acids that showed activity in the initial ATP−PP_i exchange assay with AusA was rerun in the presence of saturating amounts of one of the inhibitors (Figure 3B,C). Incubation with Phe-AMS, which inhibits A_2, eliminates the enzymatic activity with L-Phe, L-4Aph, L-Tyr, and L-Met. In the presence of Phe-AMS, AusA is capable of activating L-Val, L-Ile, L-Cle, L-Leu, L-Ala, L-Cys, and L-Tle, though the exchange rate of the second best substrate, L-Ile, is almost 10-fold lower than that with L-Val. To assess the substrate specificity of A_2, we incubated AusA with Val-AMS to inhibit A_1 and again measured the amino acid-dependent ATP−PP_i exchange rates. The activities of L-Val, L-Ile, L-Cle, L-Ala, L-Cys, L-Tle, and L-Met are eliminated. In the presence of Val-AMS, AusA is capable of activating only L-Tyr, L-Phe, L-4Aph, and L-Leu, although in all cases the activity was reduced more than 2-fold relative to the uninhibited control because of off-target inhibition of A_2 by Val-AMS.

dx.doi.org/10.1021/bi301330q | *Biochemistry* 2013, 52, 926−937

Table 4. ATP−PP_i Exchange Kinetic Parameters of AusA

entry	domain	varied substrate	nonvaried substrate	k_{cat} (min^{-1})	K_M (mM)	k_{cat}/K_M (M^{-1} s^{-1})	K_i (mM)
1	A_1	L-Val	ATP	461 ± 3	3.3 ± 0.1	2328 ± 72	NA[a]
2	A_1	L-Ile	ATP	33.9 ± 1.1	11.9 ± 0.9	47 ± 4	NA[a]
3	A_1/A_2	L-Leu	ATP	14.9 ± 1.0	24 ± 3	10.3 ± 1.5	NA[a]
4	A_2	L-Tyr	ATP	129 ± 1	1.0 ± 0	2150 ± 17	NA[a]
5	A_2	L-Phe	ATP	40.5 ± 0.6	2.1 ± 0.1	321 ± 16	NA[a]
6	A_2	L-4Aph	ATP	92 ± 2	31 ± 1	49 ± 2	NA[a]
7	A_2	ATP	L-Phe	63 ± 7	3.0 ± 0.5	350 ± 70	4.1 ± 0.7

[a]Not available.

Having established the substrate specificities of each A-domain were mutually exclusive except for L-Leu, we proceeded to examine the apparent steady-state kinetic parameters of the most active substrates using the ATP−PP_i exchange assay with AusA (Table 4). The kinetic parameters for L-Val, L-Ile, L-Leu, L-Tyr, L-Phe, and L-4Aph were determined at subsaturating concentrations of ATP because of substrate inhibition by ATP (Table 4, entry 7) and thus are reported as apparent values. The specificity constant (k_{cat}/K_M) for L-Val with A_1 is 2328 M^{-1} s^{-1}, which is 49-fold greater than that with L-Ile, the next best substrate, confirming the strict substrate specificity of A_1. Indeed, the three naturally occurring aureusimines all contain valine as the first amino acid. The k_{cat}/K_M values for L-Tyr, L-Phe, and L-4Aph with A_2 are 2150, 321, and 49 M^{-1} s^{-1}, respectively. The attenuation in k_{cat}/K_M for L-4Aph relative to that for L-Tyr is primarily due to a 31-fold increase in the K_M value for this non-natural substrate with the k_{cat} displaying a modest 30% decrease relative to the value for L-Tyr. The specificity constants for A_1 and A_2 with their optimal substrates are nearly identical, indicating a balanced activity for these two A-domains in AusA. Both A_1 and A_2 were shown to support PP_i exchange with L-Leu; thus, the kinetic parameters represent aggregate values. The k_{cat}/K_M for L-Leu is only 10 M^{-1} s^{-1}, a value more than 200-fold lower than those of the best substrates (L-Val and L-Phe) with their cognate A-domains.

Reconstitution of Aureusimine Synthetase Activity. AusA was initially expressed as the apoenzyme. To obtain a functional enzyme capable of producing aureusimine, AusA must be converted to the active holoenzyme by phosphopantetheinylation of the two thiolation domains. Ser_{947} and Ser_{1976} are predicted to be the sites of phosphopantetheinylation in T_1 and T_2, respectively. Although the aureusimine biosynthetic gene cluster encodes a dedicated phosphopantetheinyl transferase (PPTase), we elected to use Sfp, a promiscuous PPTase from *B. subtilis* that has been utilized extensively for the heterologous priming of NRPSs.[21] AusA was coexpressed with a plasmid that constitutively expresses Sfp to provide holo-AusA in yields comparable to those of the apoenzyme.

Incubation of holo-AusA (40 nM) with L-Val (25 mM), L-Phe (25 mM), NADPH (0.1 mM), and ATP (3 mM) at pH 8.0 and 37 °C led to the time-dependent formation of aureusimine-B (**2**). The reaction product comigrated via HPLC with an authentic standard that we synthesized (Supporting Information) and possessed an identical fragmentation pattern as determined by MS/MS (229.1 → 100.0). Exclusion of any of the four substrates resulted in the complete loss of aureusimine synthesis activity. These results demonstrate recombinant AusA is capable of synthesizing aureusimine-B (**2**) in vitro.

Because oxidation of the initial imine product to aureusimine-B (**2**) (Figure 1) is likely not catalyzed by AusA, we were concerned oxidative conversion to aureusimine-B (**2**) may be incomplete. As a result, we separated the reaction products from AusA using a centrifugal filter and heated the filtrate at 100 °C to promote oxidation. We conducted a time course study and found that heating the reaction filtrate for 20 min at 100 °C provided full conversion to aureusimine-B (**2**) (Figure 4). Subsequently, we detected and quantitated the

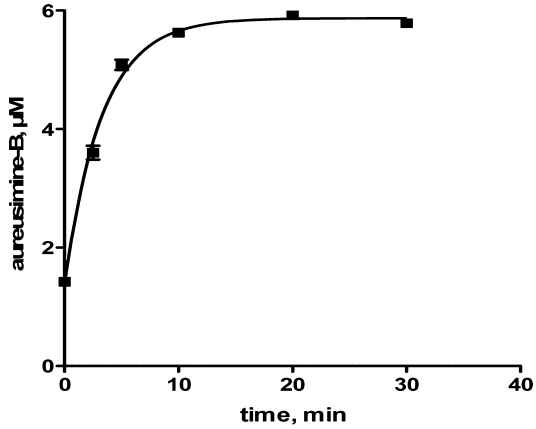

Figure 4. Thermal conversion to aureusimine-B (**2**).

pyrazinones by heating reaction filtrates for 20 min at 100 °C to ensure full conversion to the respective pyrazinone products. Zimmerman and co-workers propose oxidation of dihydroaureusimine (i.e., the imine intermediate in Figure 1) is either spontaneous or catalyzed by the reductase domain of AusA operating in reverse as an oxidoreducatase.[3] Our results suggest oxidation to aureusimine-B (**2**) is spontaneously driven by the aromatic stabilization energy of the pyrazinone.

Kinetics of Pyrazinone Formation by AusA. We evaluated the apparent kinetic parameters for pyrazinone formation for each substrate (L-Tyr, L-Val, ATP, and NADPH) at fixed saturating concentrations of the other substrates and also evaluated several additional A_2 substrates, including L-Phe, L-4Aph, and L-Leu. Finally, we examined how the kinetic parameters for ATP and NADPH change with different nonvaried A_2 substrates. We synthesized authentic standards of all pyrazinone products **1**−**4** (Supporting Information). Active site titration of AusA with Phe-AMS showed it to be ∼80% active, and the corrected concentration was used for determination of k_{cat} values (Figure S2 of the Supporting Information).

The initial rates, v_0, at a given [S] were determined by single-time point stopped-time incubation at 150 min. The reaction velocity remained linear for up to 4 h (the longest time measured). All reactions were conducted in duplicate employing a fresh enzyme preparation, and the pyrazinone products were quantified by LC−MS/MS (Materials and Methods)

dx.doi.org/10.1021/bi301330q | *Biochemistry* 2013, 52, 926−937

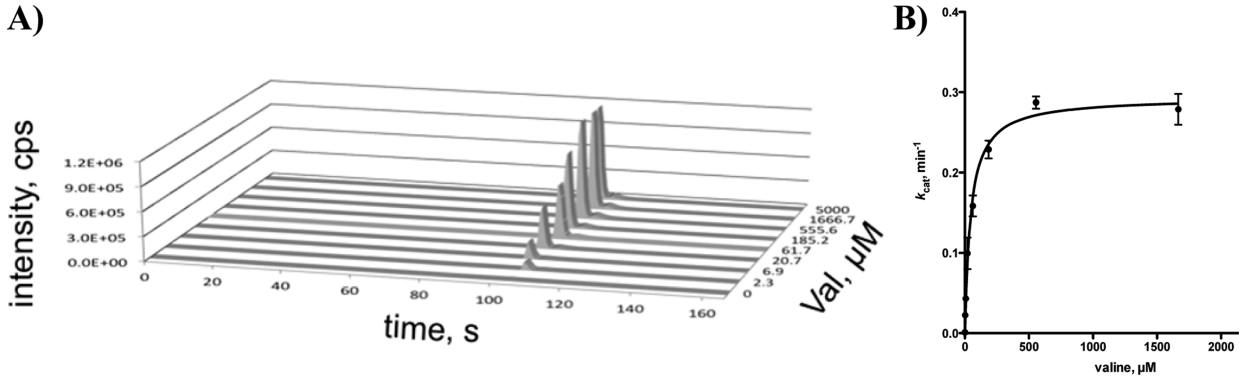

Figure 5. (A) LC−MS data for production of aureusimine-A (**1**) at varying concentrations of L-Val. (B) Normalized plot of the data shown in panel A used to determine the steady-state kinetic parameters of AusA with L-Val. Each reaction mixture contained 40 nM holo-AusA, 375 mM Bicine (pH 8.0), 10 mM $MgCl_2$, 3 mM ATP, 0.1 mM NADPH, 1 mM TCEP, 1 mM L-Tyr, and 2.3 μM to 5 mM L-Val.

Table 5. Kinetic Parameters of Pyrazinone Formation

entry	pyrazinone product	varied substrate	nonvaried substrates			k_{cat} (min^{-1})	K_M (M)	k_{cat}/K_M (M^{-1} s^{-1})	K_i (mM)
1	**1**	L-Tyr	L-Val	ATP	NADPH	0.36 ± 0.01	(1.32 ± 0.19) × 10^{-4}	45.3 ± 6.48	NA[a]
2	**2**	L-Phe	L-Val	ATP	NADPH	0.99 ± 0.04	(1.03 ± 0.14) × 10^{-3}	16.0 ± 2.26	NA[a]
3	**4**	L-4Aph	L-Val	ATP	NADPH	1.08 ± 0.04	(6.67 ± 0.66) × 10^{-3}	2.70 ± 0.28	NA[a]
4	**3**	L-Leu	L-Val	ATP	NADPH	1.32 ± 0.46	(1.49 ± 0.60) × 10^{-1}	0.15 ± 0.08	NA[a]
5	**1**	L-Val	L-Tyr	ATP	NADPH	0.39 ± 0.02	(5.03 ± 0.70) × 10^{-5}	130 ± 19.0	NA[a]
6	**1**	ATP	L-Val	L-Tyr	NADPH	0.39 ± 0.02	(1.04 ± 0.15) × 10^{-4}	62.5 ± 9.32	NA[a]
7	**2**	ATP	L-Val	L-Phe	NADPH	1.22 ± 0.15	(4.55 ± 1.42) × 10^{-4}	44.8 ± 15.0	NA[a]
8	**4**	ATP	L-Val	L-4Aph	NADPH	0.90 ± 0.09	(1.12 ± 0.23) × 10^{-3}	13.3 ± 3.00	NA[a]
9	**3**	ATP	L-Val	L-Leu	NADPH	1.32 ± 0.63	(9.73 ± 5.51) × 10^{-3}	2.26 ± 1.67	3.53 ± 2.21
10	**1**	NADPH	L-Val	L-Tyr	ATP	0.71 ± 0.05	(2.15 ± 0.40) × 10^{-5}	551 ± 110	2.16 ± 0.68
11	**2**	NADPH	L-Val	L-Phe	ATP	1.53 ± 0.08	(1.68 ± 0.29) × 10^{-5}	1510 ± 272	9.70 ± 8.00
12	**4**	NADPH	L-Val	L-4Aph	ATP	1.30 ± 0.08	(1.18 ± 0.23) × 10^{-5}	1830 ± 381	2.04 ± 0.65
13	**3**	NADPH	L-Val	L-Leu	ATP	0.38 ± 0.02	(5.12 ± 1.15) × 10^{-6}	1220 ± 284	1.84 ± 0.61

[a]Not available.

employing a standard curve generated from our synthetic standards. Apparent steady-state kinetic parameters were determined by fitting the v_0 versus [S] plots to the Michaelis−Menten equation (eq 1, Materials and Methods) or substrate inhibition model (eq 2, Materials and Methods). Representative LC−MS data and the corresponding saturation curve for determination of the steady-state kinetic parameters for L-Val are shown in Figure 5. Initial velocity experiments provided K_M values of 132, 50, 104, and 22 μM for L-Tyr, L-Val, ATP, and NADPH, respectively, with an average k_{cat} of 0.38 ± 0.01 min^{-1} for L-Val, L-Tyr, and ATP (Table 5, entries 1, 5, 6, and 10). The k_{cat} of 0.71 min^{-1} using NADPH as the varied substrate is a result of fitting the saturation curve to the substrate inhibition model, which showed NADPH exhibits substrate inhibition with a K_i of 2.2 mM. Notably, at 0.1 mM NADPH (the concentration employed when NADPH was the nonvaried substrate), the k_{obs} is 0.39 min^{-1}, consistent with the other values.

Because of the relaxed substrate specificity of A_2, we evaluated L-Phe, L-4Aph, and L-Leu (Table 5, entries 2−4, respectively) with fixed saturating concentrations of L-Val, ATP, and NADPH and observed formation of the pyrazinones **2**−**4**, respectively. The k_{cat}/K_M values for L-Phe, L-4Aph, and L-Leu are 2.8-, 17-, and 302-fold lower, respectively, than that of L-Tyr, which is the best A_2 substrate. The 2.8-fold difference in k_{cat}/K_M for L-Tyr and L-Phe almost precisely matches the 3:1 observed product ratio of aureusimine-A (**1**) to aureusimine-B (**2**).[2] The decrease in k_{cat}/K_M is driven exclusively by an increase in K_M values for L-Phe, L-4Aph, and L-Leu as all three substrates exhibit approximately 3-fold greater k_{cat} values. Surprisingly, despite being an extremely poor substrate for A_2, L-Leu is incorporated into aureusimine-C (**3**), demonstrating that this substrate is efficiently processed by the downstream C and R domains.[3] Although direct comparison of exchange kinetics and steady-state turnover kinetics is not valid, we did observe close correlation in the k_{cat}/K_M values. This suggests the ATP−PP_i exchange assay, commonly used to assess A-domain substrate specificity, is an excellent surrogate for the overall complete NRPS reaction. By contrast, the K_M values obtained from the ATP−PP_i exchange assay were up to 60-fold higher than those observed in the product formation assay. The k_{cat} value in the product formation assay for L-Tyr is the lowest of all A_2 substrates examined, which was unexpected because L-Tyr displays the highest k_{cat} in the ATP−PP_i exchange assay. This indicates that transfer of the tyrosinyl-AMP intermediate to T_2, condensation with L-Val~S-T_2, or the reductive release of the final product is much slower than with L-Phe or the other substrates.

When ATP was examined as the varied substrate at fixed concentrations of L-Val and NADPH, but employing different A_2 substrates [L-Tyr, L-Phe, L-4Aph, and L-Leu (Table 5, entries 6−9, respectively)], the observed K_M values ranged from 0.1 mM (with L-Tyr as the nonvaried amino acid) to 9.7 mM (with L-Leu as the nonvaried amino acid). The K_M values for ATP thus vary over 2 orders of magnitude and parallel the trend in amino acid K_M values. This is expected because the amino acid

dx.doi.org/10.1021/bi301330q | *Biochemistry* 2013, 52, 926−937

and ATP are linked through the kinetic mechanism, in which binding of the amino acid drives binding of ATP through formation of the acyl adenylate and further downstream central complexes. Because ATP is abundant, estimated to be present at a concentration of 3 mM in cells, these differences in K_M values may be less important in vivo.[22] When NADPH was examined as the varied substrate at fixed concentrations of L-Val and ATP, but employing different A_2 substrates [L-Tyr, L-Phe, L-4Aph, and L-Leu (Table 5, entries 10−13, respectively)], the ranges of K_M and k_{cat}/K_M values were less than 5-fold.

Reductive Release. The reductase domain in AusA is a member of the short chain dehydrogenase/reductase (SDR) enzyme superfamily and contains the signature YXXXK catalytic motif as well as a Rossman fold for NADPH binding (Figure S3 of the Supporting Information). AusA exhibits strict cofactor specificity for NADPH and is unable to use NADH (data not shown). To further assess the R-domain specificity and kinetics, we employed a continuous kinetic assay to monitor consumption of NADPH by a decrease in absorbance at 360 nm (Materials and Methods). Incubation of AusA with all substrates and cofactors (L-Val, L-Tyr, NADPH, and ATP) resulted in a time-dependent decrease in the concentration of NADPH corresponding to 2.01 min^{-1} (Table 6, entry 1). The

Table 6. NADPH Consumption Assay

entry	substrates	NADPH consumption k_{obs} (min^{-1})	aureusimine-A formation k_{obs} (min^{-1})
1	L-Val, L-Tyr, ATP, NADPH	2.01 ± 0.05	0.28 ± 0.01
2	L-Val, ATP, NADPH	0	0
3	L-Tyr, ATP, NADPH	1.64 ± 0.01	0

rate of aureusimine-A (**1**) production (k_{obs}) under these conditions is 0.28 min^{-1} (Table 6, entry 1). To understand the origin of the substantially higher rate of NADPH consumption relative to the rate of product formation, we then performed the assay under otherwise identical conditions, but excluding either L-Val or L-Tyr. In the absence of L-Tyr, we did not observe any NADPH consumption (Table 6, entry 2). However, in the absence of L-Val, we unexpectedly observed substantial NADPH consumption with a k_{obs} of 1.64 min^{-1} (Table 6, entry 3). These results indicate the R-domain is able to rapidly turn over L-Tyr, presumably to the corresponding aldehyde (i.e., tyrosinal) or alcohol (i.e., tyrosinol). To confirm the turnover products, we synthesized authentic standards of tyrosinol and a stabile oxime derivative of tyrosinal (see the Supporting Information). Because tyrosinal is unstabile, the reaction products were directly treated with pentafluorobenzyl hydroxylamine to form a tyrosinal oxime derivative (Materials and Methods). LC−MS confirmed that L-Tyr is reduced to tyrosinal but not further reduced to tyrosinol. We then excluded ATP from the reaction mixture or added the A_2-specific inhibitor Phe-AMS to demonstrate L-Tyr must be activated by A_2 and tethered to T_2. In both cases, consumption of NADPH was not observed (data not shown). Taken together, these results confirm L-Tyr must be activated by A_2 to undergo reduction and show the R-domain is able to turn over L-Tyr-S∼T_2 much more rapidly than the dipeptidyl substrate L-Val-L-Tyr-S∼T_2. These results in turn suggest dipeptide formation catalyzed by the C-domain is substantially slower than reductive release because the partition ratio of products (reduced tyrosine products vs cyclized dipeptides) is reflective of T_2 occupancy. Finally, we note the observed consumption of NADPH with all substrates (k_{obs} = 2.01 min^{-1}) is nearly equal to the sum of the observed rates of aureusimine-A (**1**) formation (k_{obs} = 0.28 min^{-1}) and tyrosine turnover (k_{obs} = 1.64 min^{-1}).

DISCUSSION

Pyrazinones are relatively rare heterocyles in natural products, and their reported activities range from antibacterial for simple 3,6-disubstituted analogues to antiviral for the more complex (bis)indole alkaloids. The naturally occurring 3,6-disubstituted pyrazinones include argvalin,[23] arglecin,[24] OPC-15161,[25] flavacol and related hydroxylated metabolites,[26] several 1-hydroxypyrazinones,[27] peramine,[28] and the (bis)indole alkaloid dragmacidins.[29] Aureusimine-B was previously isolated from a *Streptomyces* sp., and although no antibacterial activity was observed, it was shown to inhibit calpain, a serine protease with modest activity (∼1 μM).[30]

A related dipeptide-derived class of natural products includes the diketopiperazines (DKPs), which can be produced nonribosomally or by cyclodipeptide synthases.[31] NRPS-mediated synthesis of DKPs typically uses a dimodule similar to AusA, but lacking a C-terminal domain to catalyze peptide release. In the absence of a C-terminal release domain, cyclization to afford a DKP generally occurs spontaneously, especially when proline is present as the first amino acid. The structurally related pyrazines are another important class of natural products. On the basis of the chemical precedence of Sperry and Badrinarayanan[32] and recent biochemical characterization by Tang and co-workers of a fungal NRPS,[33] it seems plausible that 2,5-disubstituted symmetrical pyrazines of bacterial and fungal origin may employ a similar biosynthetic logic using a NRPS with the C−A−T−R architecture to convert an amino acid to an amino aldehyde. Spontaneous dimerization of the amino aldehyde and subsequent oxidation would provide the pyrazine derivative. Dimerization may alternatively be enzyme-catalyzed, as observed during the biosynthesis of saframycin by the monomodular NRPS SfmC.[34]

We utilized a novel strategy to assess the substrate specificity of each A-domain within the context of full-length AusA using selective A-domain acyl adenylate mimics (Val-AMS for A_1 and Phe-AMS for A_2) to inhibit the other A-domain. Previous characterization of NRPSs with multiple A-domains has been performed primarily through excision of each A-domain from the NRPS and expression as a stand-alone protein. This not only limits kinetic evaluation to the adenylate-forming half-reaction but also prohibits characterization of the A-domain in its normal context where protein−protein interactions may modulate activity. Walsh and Balibar characterized the trimodular NRPS GliP involved in gliotoxin biosynthesis that contains two A-domains by separately mutating the conserved aspartic residue in each A-domain active site that ion-pairs with the amine of the amino acid substrate.[35] The resulting mutation abolished A-domain activity and allowed kinetic evaluation in the context of the large trimodular NRPS. Another technique for characterizing A-domain substrate specificity was reported by Kelleher and co-workers and involves direct characterization of the loaded substrate on the cognate T-domain using Fourier transform mass spectrometry.[36] Our strategy employing A-domain inhibitors provides a complementary method for characterizing A-domain specificity in multidomain NRPSs containing more than one A-domain. A limitation is that it

dx.doi.org/10.1021/bi301330q | *Biochemistry* 2013, 52, 926−937

requires a priori knowledge of the substrate specificity from bioinformatic analysis.

AusA uses a reductase (R) domain for release of a dipeptidyl aldehyde that reacts intramolecularly with the N-terminus to afford a six-membered imine, which spontaneously oxidizes to the final pyrazinone product. Interestingly, the $A_1-T_1-C-T_2-A_2-R$ domain architecture of AusA is found in the NRPS genes involved in the biosynthesis of the benzodiazepine anthramycin, but the loading and extension modules are separate proteins.[37] The R-domain in the anthramycin NRPS is also predicted to catalyze a two-electron reductive release to afford an aldehyde, which undergoes spontaneous condensation with an internal amine to afford a seven-membered hemiaminal. However, the resultant hemiaminal in anthramycin biosynthesis does not dehydrate to an imine, likely as a result of ring strain. In the absence of an internal nucleophile to rapidly capture the product aldehyde, further reduction to an alcohol is favored (an overall four-electron reduction) because aldehydes are more reactive than thioesters. This is illustrated in the R-domain-catalyzed four-electron reductive release of lyngbyatoxin,[38] myxochelin,[16] and mycobacterial glycopeptidolipids,[39] all of which lack appropriately positioned hydroxy or amino groups to intramolecularly condense with the intermediate aldehyde.[11] Gokahle and co-workers demonstrated aldehyde reduction is approximately 10 times faster than thioester reduction during their study of the R-domain involved in reductive release of the mycobacterial glycopeptidolipids. The mechanism for reduction is nonprocessive, requiring the initially formed aldehyde product to dissociate from the enzyme to allow for cofactor exchange of NAD(P) for NAD(P)H. Rebinding of aldehyde followed by a second reduction provides the primary alcohol final product.[39]

The in vitro reconstitution of complete NRPS pathways[40] has been reported for only a handful of natural products, including cyclooctadepsipeptide PF1022,[41,42] pacidamycin,[43] antimycin,[44] beauvericins,[45] and the siderophore synthesis pathways involved in production of enterobactin,[46] yersiniabactin,[47] pyochelin,[48] vibriobactin,[49] myxochelin,[16] and pseudomonine.[50] Biosynthesis of the indole alkaloid terrequinone, which uses a noncanonical monomodular NRPS for dimerization of a tryptophan derivative, was also reconstituted in vitro.[51,52] A focus of many earlier studies was uncovering novel enzyme activities as well as providing fundamental insight into the logic of NRPS biosynthesis, often using single-turnover experiments employing radiolabeled substrates. The only available k_{cat} values for the formation of product from fully reconstituted native pathways are those for enterobactin, yersiniabactin, and pyochelin, and these range from 1.4 min^{-1} for yersiniabactin[46] to 140 min^{-1} for enterobactin.[46] Stachelhaus and Hahn have also reported the reconstitution of two excised NRPS modules from the tyrocidin NRPS pathway that produced a diketopiperazine with a k_{obs} of 0.94 min^{-1}.[53] Surprisingly, K_M values for small molecule substrates and cofactors determined by measuring product formation have been reported only for salicylic acid in the synthesis of yersiniabactin.[46]

The lack of Michaelis–Menten kinetic parameters with respect to product formation can be attributed to several factors, including the lack of assay sensitivity, product inhibition, and/or the complexity of the multiprotein systems. Consequently, the results obtained herein that provide simple steady-state kinetic parameters (Table 5) of all substrates and cofactors, including non-natural substrates involved in pyrazinone formation, are notable. We found the K_M values for the amino acid substrates were up to 60-fold lower in the product formation than in the classic ATP–PP_i exchange assay that is most commonly used to assess A-domain substrate specificity. Significantly, the K_M value for ATP in the product formation assay changed more than 100-fold depending on the amino acid employed. While this result is readily reconciled because the amino acid and ATP are kinetically linked through acyl adenylate formation, it highlights the importance of a more careful examination of reaction kinetics. We believe the kinetic parameters obtained herein provide a useful foundation for future studies using AusA as a model NRPS and highlight the utility of this simple dimodular NRPS for kinetic characterization.

■ ASSOCIATED CONTENT

Supporting Information

Synthesis of pyrazinones **1**–**4**, Val-AMS **5**, Phe-AMS **6**, tyrosinol **S8**, and tyrosinal oxime **S10**; alignment and homology model of the A_1 domain of AusA; active site titration of AusA; alignment of the R-domain; and saturation curves for all substrates listed in Tables 4 and 5. This material is available free of charge via the Internet at http://pubs.acs.org.

■ AUTHOR INFORMATION

Corresponding Author

*Phone: (612) 625-7956. Fax: (612) 626-5173. E-mail: aldri015@umn.edu.

Funding

We gratefully acknowledge National Institutes of Health Grants GM-068440 (to A.M.G.) and AI-070219 (to C.C.A.).

Notes

The authors declare no competing financial interest.

■ ACKNOWLEDGMENTS

We thank Mrs. Kathryn Nelson for carefully proofreading the manuscript and Prof. David H. Sherman (University of Michigan, Ann Arbor, MI) for generously providing plasmid pSFP.

■ ABBREVIATIONS

A-domain, adenylation domain; L-4Aph, L-4-aminophenylalanine; β-Phe, β-aminophenylalanine; C-domain, condensation domain; L-Cle, L-cycloleucine; Mpa, α-methylphenylalanine; NRP, nonribosomal peptide; NRPS, nonribosomal peptide synthetase; Phe-AMS, 5′-*O*-[*N*-(phenylalanyl)sulfamoyl]-adenosine; R-domain, reductase domain; T-domain, thiolation domain; TE, thioesterase; L-Tle, L-*tert*-leucine; Val-AMS, 5′-*O*-[*N*-(valinyl)sulfamoyl]adenosine.

■ REFERENCES

(1) David, M. Z., and Daum, R. S. (2010) Community-associated methicillin-resistant *Staphylococcus aureus*: Epidemiology and clinical consequences of an emerging epidemic. *Clin. Microbiol. Rev. 23*, 616–687.

(2) Wyatt, M. A., Wang, W., Roux, C. M., Beasley, F. C., Heinrichs, D. E., Dunman, P. M., and Magarvey, N. A. (2010) *Staphylococcus aureus* nonribosomal peptide secondary metabolites regulate virulence. *Science 329*, 294–296.

(3) Zimmermann, M., and Fischbach, M. A. (2010) A family of pyrazinone natural products from a conserved nonribosomal peptide synthetase in *Staphylococcus aureus*. *Chem. Biol. 17*, 925–930.

(4) Wyatt, M. A., Wang, W., Roux, C. M., Beasley, F. C., Heinrichs, D. E., Dunman, P. M., and Magarvey, N. A. (2011) Clarification of "*Staphylococcus aureus* nonribosomal peptide secondary metabolites regulate virulence". *Science 333*, 1381.
(5) Sun, F., Cho, H., Jeong, D. W., Li, C., He, C., and Bae, T. (2010) Aureusimines in *Staphylococcus aureus* are not involved in virulence. *PLoS One 5*, e15703.
(6) Secor, P. R., Jennings, L. K., James, G. A., Kirker, K. R., Pulcini, E. D., McInnerney, K., Gerlach, R., Livinghouse, T., Hilmer, J. K., Bothner, B., Fleckman, P., Olerud, J. E., and Stewart, P. S. (2012) Phevalin (aureusimine B) production by *Staphylococcus aureus* biofilm and impacts on human keratinocyte gene expression. *PLoS One 7*, e40973.
(7) Sieber, S. A., and Marahiel, M. A. (2005) Molecular mechanisms underlying nonribosomal peptide synthesis: Approaches to new antibiotics. *Chem. Rev. 105*, 715−738.
(8) Fischbach, M. A., and Walsh, C. T. (2006) Assembly-line enzymology for polyketide and nonribosomal peptide antibiotics: Logic, machinery, and mechanisms. *Chem. Rev. 106*, 3468−3496.
(9) Gulick, A. M. (2009) Conformational dynamics in the acyl-CoA synthetases, adenylation domains of non-ribosomal peptide synthetases, and firefly luciferase. *ACS Chem. Biol. 4*, 811−827.
(10) Mercer, A. C., and Burkart, M. D. (2007) The ubiquitous carrier protein: A window to metabolite biosynthesis. *Nat. Prod. Rep. 24*, 750−773.
(11) Du, L., and Lou, L. (2010) PKS and NRPS release mechanisms. *Nat. Prod. Rep. 27*, 255−278.
(12) Edwards, D. J., and Gerwick, W. H. (2004) Lyngbyatoxin biosynthesis: Sequence of biosynthetic gene cluster and identification of a novel aromatic prenyltransferase. *J. Am. Chem. Soc. 126*, 11432−11433.
(13) Yin, W. B., Grundmann, A., Cheng, J., and Li, S. M. (2009) Acetylaszonalenin biosynthesis in *Neosartorya fischeri*. Identification of the biosynthetic gene cluster by genomic mining and functional proof of the genes by biochemical investigation. *J. Biol. Chem. 284*, 100−109.
(14) Maiya, S., Grundmann, A., Li, S. M., and Turner, G. (2006) The fumitremorgin gene cluster of *Aspergillus fumigatus*: Identification of a gene encoding brevianamide F synthetase. *ChemBioChem 7*, 1062−1069.
(15) Wyatt, M. A., Mok, M. C., Junop, M., and Magarvey, N. A. (2012) Heterologous expression and structural characterisation of a pyrazinone natural product assembly line. *ChemBioChem 13*, 2408−2415.
(16) Li, Y., Weissman, K. J., and Muller, R. (2008) Myxochelin biosynthesis: Direct evidence for two- and four-electron reduction of a carrier protein-bound thioester. *J. Am. Chem. Soc. 130*, 7554−7555.
(17) Vondenhoff, G. H., and Van Aerschot, A. (2011) Aminoacyl-tRNA synthetase inhibitors as potential antibiotics. *Eur. J. Med. Chem. 46*, 5227−5236.
(18) Francklyn, C. S., First, E. A., Perona, J. J., and Hou, Y. M. (2008) Methods for kinetic and thermodynamic analysis of aminoacyl-tRNA synthetases. *Methods 44*, 100−118.
(19) Copeland, R. A. (2005) Tight Binding Inhibitors. In *Evaluation of Enzyme Inhibitors in Drug Discovery: A Guide for Medicinal Chemists and Pharmacologists*, pp 178−213, Wiley, Hoboken, NJ.
(20) Mitchell, C. A., Shi, C., Aldrich, C. C., and Gulick, A. M. (2012) Structure of PA1221, a nonribosomal peptide synthetase containing adenylation and peptidyl carrier protein domains. *Biochemistry 51*, 3252−3263.
(21) Quadri, L. E., Weinreb, P. H., Lei, M., Nakano, M. M., Zuber, P., and Walsh, C. T. (1998) Characterization of Sfp, a *Bacillus subtilis* phosphopantetheinyl transferase for peptidyl carrier protein domains in peptide synthetases. *Biochemistry 37*, 1585−1595.
(22) Neuhard, J., and Nygaard, P. (1987) *Escherichia coli* and *Salmonella typhimurium*. In *Cellular and Molecular Biology*, Vol. *1*, pp 445−473, ASM Press, Washington, DC.
(23) Tatsuta, K., Fujimoto, K., Yamashita, M., Tsuchiya, T., and Umezawa, S. (1973) Argvalin, a new microbial metabolite: Isolation and structure. *J. Antibiot. 26*, 606−608.
(24) Tatsuta, K., Tsuchiya, T., Umezawa, S., Naganawa, H., and Umezawa, H. (1972) Revised structure for arglecin. *J. Antibiot. 25*, 674−676.
(25) Nakano, Y., Kawaguchi, T., Sumitomo, J., Takizawa, T., Uetsuki, S., Sugawara, M., and Kido, M. (1991) Novel inhibitors of superoxide anion generation, OPC-15160 and OPC-15161. Taxonomy, fermentation, isolation, physico-chemical properties, biological characteristics and structure determination. *J. Antibiot. 44*, 52−58.
(26) Yamazaki, M., Maebayashi, Y., and Miyaki, K. (1972) Isolation of a new type of pyrazine metabolite from *Aspergillus ochraceus* WILH. *Chem. Pharm. Bull. 20*, 2274−2276.
(27) MacDonald, J. C. (1972) New analogues of aspergillic acid derived from methionine. *Can. J. Biochem. 50*, 543−549.
(28) Rowan, D. D., Hunt, M. B., and Gaynor, D. L. (1986) Peramine, a novel insect feeding deterrent from ryegrass infected with the endophyte *Acremonium loliae*. *J. Chem. Soc., Chem. Commun.*, 935−936.
(29) Capon, R. J., Rooney, F., Murray, L. M., Collins, E., Sim, A. T. R., Rostas, J. A. P., Butler, M. S., and Carroll, A. R. (1998) Dragmacidins: New protein phosphatase inhibitors from a southern Australian deep-water marine sponge, *Spongosorites* sp. *J. Nat. Prod. 61*, 660−662.
(30) Alvarez, M. E., White, C. B., Gregory, J., Kydd, G. C., Harris, A., Sun, H. H., Gillum, A. M., and Cooper, R. (1995) Phevalin, a new calpain inhibitor, from a *Streptomyces* sp. *J. Antibiot. 48*, 1165−1167.
(31) Belin, P., Moutiez, M., Lautru, S., Seguin, J., Pernodet, J. L., and Gondry, M. (2012) The nonribosomal synthesis of diketopiperazines in tRNA-dependent cyclodipeptide synthase pathways. *Nat. Prod. Rep. 29*, 961−979.
(32) Badrinarayanan, S., and Sperry, J. (2012) Pyrazine alkaloids via dimerization of amino acid-derived α-amino aldehydes: Biomimetic synthesis of 2,5-diisopropylpyrazine, 2,5-bis(3-indolylmethyl)pyrazine and actinopolymorphol C. *Org. Biomol. Chem. 10*, 2126−2132.
(33) Qiao, K., Zhou, H., Xu, W., Zhang, W., Garg, N., and Tang, Y. (2011) A fungal nonribosomal peptide synthetase module that can synthesize thiopyrazines. *Org. Lett. 13*, 1758−1761.
(34) Koketsu, K., Watanabe, K., Suda, H., Oguri, H., and Oikawa, H. (2010) Reconstruction of the saframycin core scaffold defines dual Pictet-Spengler mechanisms. *Nat. Chem. Biol. 6*, 408−410.
(35) Balibar, C. J., and Walsh, C. T. (2006) GliP, a multimodular nonribosomal peptide synthetase in *Aspergillus fumigatus*, makes the diketopiperazine scaffold of gliotoxin. *Biochemistry 45*, 15029−15038.
(36) Dorrestein, P. C., Blackhall, J., Straight, P. D., Fischbach, M. A., Garneau-Tsodikova, S., Edwards, D. J., McLaughlin, S., Lin, M., Gerwick, W. H., Kolter, R., Walsh, C. T., and Kelleher, N. L. (2006) Activity screening of carrier domains within nonribosomal peptide synthetases using complex substrate mixtures and large molecule mass spectrometry. *Biochemistry 45*, 1537−1546.
(37) Hu, Y., Phelan, V., Ntai, I., Farnet, C. M., Zazopoulos, E., and Bachmann, B. O. (2007) Benzodiazepine biosynthesis in *Streptomyces refuineus*. *Chem. Biol. 14*, 691−701.
(38) Read, J. A., and Walsh, C. T. (2007) The lyngbyatoxin biosynthetic assembly line: Chain release by four-electron reduction of a dipeptidyl thioester to the corresponding alcohol. *J. Am. Chem. Soc. 129*, 15762−15763.
(39) Chhabra, A., Haque, A. S., Pal, R. K., Goyal, A., Rai, R., Joshi, S., Panjikar, S., Pasha, S., Sankaranarayanan, R., and Gokhale, R. S. (2012) Nonprocessive [2 + 2]e^- off-loading reductase domains from mycobacterial nonribosomal peptide synthetases. *Proc. Natl. Acad. Sci. U.S.A. 109*, 5681−5686.
(40) Sattely, E. S., Fischbach, M. A., and Walsh, C. T. (2008) Total biosynthesis: In vitro reconstitution of polyketide and nonribosomal peptide pathways. *Nat. Prod. Rep. 25*, 757−793.
(41) Feifel, S. C., Schmiederer, T., Hornbogen, T., Berg, H., Sussmuth, R. D., and Zocher, R. (2007) In vitro synthesis of new enniatins: Probing the α-D-hydroxy carboxylic acid binding pocket of the multienzyme enniatin synthetase. *ChemBioChem 8*, 1767−1770.
(42) Muller, J., Feifel, S. C., Schmiederer, T., Zocher, R., and Sussmuth, R. D. (2009) In vitro synthesis of new cyclodepsipeptides of

the PF1022-type: Probing the α-D-hydroxy acid tolerance of PF1022 synthetase. *ChemBioChem 10*, 323−328.
(43) Zhang, W., Ntai, I., Bolla, M. L., Malcolmson, S. J., Kahne, D., Kelleher, N. L., and Walsh, C. T. (2011) Nine enzymes are required for assembly of the pacidamycin group of peptidyl nucleoside antibiotics. *J. Am. Chem. Soc. 133*, 5240−5243.
(44) Sandy, M., Rui, Z., Gallagher, J., and Zhang, W. (2012) Enzymatic synthesis of dilactone scaffold of antimycins. *ACS Chem. Biol. 7*, 1956−1961.
(45) Matthes, D., Richter, L., Muller, J., Denisiuk, A., Feifel, S. C., Xu, Y., Espinosa-Artiles, P., Sussmuth, R. D., and Molnar, I. (2012) In vitro chemoenzymatic and in vivo biocatalytic syntheses of new beauvericin analogues. *Chem. Commun. 48*, 5674−5676.
(46) Gehring, A. M., Mori, I., and Walsh, C. T. (1998) Reconstitution and characterization of the *Escherichia coli* enterobactin synthetase from EntB, EntE, and EntF. *Biochemistry 37*, 2648−2659.
(47) Miller, D. A., Luo, L., Hillson, N., Keating, T. A., and Walsh, C. T. (2002) Yersiniabactin synthetase: A four-protein assembly line producing the nonribosomal peptide/polyketide hybrid siderophore of *Yersinia pestis*. *Chem. Biol. 9*, 333−344.
(48) Patel, H. M., and Walsh, C. T. (2001) In vitro reconstitution of the *Pseudomonas aeruginosa* nonribosomal peptide synthesis of pyochelin: Characterization of backbone tailoring thiazoline reductase and N-methyltransferase activities. *Biochemistry 40*, 9023−9031.
(49) Keating, T. A., Marshall, C. G., and Walsh, C. T. (2000) Reconstitution and characterization of the *Vibrio cholerae* vibriobactin synthetase from VibB, VibE, VibF, and VibH. *Biochemistry 39*, 15522−15530.
(50) Sattely, E. S., and Walsh, C. T. (2008) A latent oxazoline electrophile for N-O-C bond formation in pseudomonine biosynthesis. *J. Am. Chem. Soc. 130*, 12282−12284.
(51) Schneider, P., Weber, M., Rosenberger, K., and Hoffmeister, D. (2007) A one-pot chemoenzymatic synthesis for the universal precursor of antidiabetes and antiviral bis-indolylquinones. *Chem. Biol. 14*, 635−644.
(52) Balibar, C. J., Howard-Jones, A. R., and Walsh, C. T. (2007) Terrequinone A biosynthesis through L-tryptophan oxidation, dimerization and bisprenylation. *Nat. Chem. Biol. 3*, 584−592.
(53) Hahn, M., and Stachelhaus, T. (2004) Selective interaction between nonribosomal peptide synthetases is facilitated by short communication-mediating domains. *Proc. Natl. Acad. Sci. U.S.A. 101*, 15585−15590.